ELSEVIER

Computers & Geosciences 32 (2006) 259–264

COMPUTERS & GEOSCIENCES

www.elsevier.com/locate/cageo

An efficient Matlab script to calculate heterogeneous anisotropically elastic wave propagation in three dimensions ☆

Oliver S. Boyd*

University of Colorado at Boulder, USA

Received 1 March 2005; received in revised form 17 June 2005; accepted 20 June 2005

Abstract

We have created a second-order finite-difference solution to the anisotropic elastic wave equation in three dimensions and implemented the solution as an efficient Matlab script. This program allows the user to generate synthetic seismograms for three-dimensional anisotropic earth structure. The code was written for teleseismic wave propagation in the 1–0.1 Hz frequency range but is of general utility and can be used at all scales of space and time. This program was created to help distinguish among various types of lithospheric structure given the uneven distribution of sources and receivers commonly utilized in passive source seismology. Several successful implementations have resulted in a better appreciation for subduction zone structure, the fate of a transform fault with depth, lithospheric delamination, and the effects of wavefield focusing and defocusing on attenuation. Companion scripts are provided which help the user prepare input to the finite-difference solution. Boundary conditions including specification of the initial wavefield, absorption and two types of reflection are available.

Keywords: Seismology; Synthetics; Receiver function; Anisotropy; Finite-difference

1. Introduction

The advent of affordable personal computing systems has made the calculation of three-dimensional finite-difference synthetic seismograms a reasonable endeavor. Analytic solutions to the elastic wave equation are confined to simple problems, usually a set of flat layers (Frederiksen and Bostock, 1999). Finite-difference solutions, however, allow a fully arbitrary model to be specified (Bohlen, 2002; Igel et al., 1995; Juhlin, 1995; Kelly et al., 1976; Levander, 1988). This advantage provides for a full set of surface multiples, focusing and defocusing of seismic waves, wave front healing, and complex frequency-dependent effects to be observed. One disadvantage of the numerical finite-difference approach is the production of artifacts resulting from numerical instability and imperfect boundary conditions.

We have produced a second-order finite-difference solution to the anisotropic elastic wave equation. This solution is implemented as a Matlab script, which has the advantage of enabling the user to interrogate and change variables during runtime. For example, the wavefield as a function of time can be observed allowing the seismologist to determine how a particular arrival was produced. We have verified our solution by comparison with analytic methods.

☆Code on server at http://www.iamg.org/CGEditor/index.htm

*Corresponding author at: US Geological Survey, Geological Hazards Team, MS 966, Box 25046, Denver CO 80225, USA. Tel.: +1 30 32738571; fax: +1 30 32738600.

E-mail address: olboyd@usgs.gov.

0098-3004/$ - see front matter © 2005 Elsevier Ltd. All rights reserved.
doi:10.1016/j.cageo.2005.06.019

2. Method

The seismic wave equation is derived from setting the acceleration of a given mass with density ρ, the second derivative of its position, u, with respect to time, t, equal to the forces acting on that mass (Shearer, 1999). These forces include body forces, f_i, such as gravity as well as normal and tangential stresses that act on the surface of the mass:

$$\rho \frac{\partial^2 \mu_i}{\partial t^2} = \sum_{j=1,3} \frac{\partial \tau_{ij}}{\partial x_j} + f_i. \tag{1}$$

The subscripts i and j refer to the coordinate directions, e.g. x, y, and z, u is displacement, t is time, and x is a spatial dimension. The stress, τ, must be expressed in terms of the displacement. The anisotropic stress–displacement relationship is (Babuska and Cara, 1991)

$$\tau_{ij} = c_{ijkl} \frac{1}{2} (\partial_l u_k + \partial_k u_l), \tag{2}$$

where c_{ijkl} is the fourth-order stiffness tensor having 21 independent elastic coefficients for an arbitrary anisotropic medium.

Upon substitution of (2) into (1), a set of first- and second-order derivatives are produced. The second-order finite-difference solution for the first and second spatial derivatives of displacement are

$$\frac{\partial u}{\partial x} = \frac{u_{i+1} - u_{i-1}}{2\,\mathrm{d}x}, \tag{3}$$

$$\frac{\partial^2 u}{\partial x^2} = \frac{u_{i+1} - 2u_i + u_{i-1}}{\mathrm{d}x^2}. \tag{4}$$

Spatial derivatives of c_{ijkl} are obtained in the same fashion. The second-order temporal derivative is analogous to Eq. (4) where x is replaced by t and i by a temporal index, n. We then solve for u_{n+1}, which results in the second order finite-difference solution to the anisotropic wave equation for displacement.

To maintain numerical stability, the temporal spacing should adhere to the following formula:

$$\mathrm{d}t \leq \frac{\mathrm{d}x}{\sqrt{\mu/\rho + (\lambda + 2\mu)/\rho}}, \tag{5}$$

where μ and λ are the Lamé parameters (Kelly et al., 1976). The first (second) term in the denominator is the square of the isotropic S-wave (P-wave) velocity. These terms should reflect the largest seismic velocities allowable by the stiffness tensors used in the model. To minimize dispersion, the grid spacing should be less than one-tenth of the wavelength at the upper half-power frequency (Kelly et al., 1976), this time considering the minimum seismic velocity. Dispersion can also be reduced by using a higher-order spatial derivative (Levander, 1988), but that method is not implemented here.

Additional problems can result from artifacts generated by the boundary conditions. This is mitigated by increasing the width of the model domain or using some type of absorbing boundary. We employ the absorbing boundary developed by Higdon (1991). The displacement on the boundary is expressed as a function of neighboring displacements, time, and seismic velocities,

$$u_{t+1} = -q_x u_{t+1,2} - q_t u_{t,1} - q_{tx} u_{t,2}, \tag{6}$$

where

$$\begin{aligned} q_x &= \frac{b(B+V) - V}{(B+V)(1-b)}, \\ q_t &= \frac{b(B+V) - B}{(B+V)(1-b)}, \\ q_{tx} &= \frac{b}{b-1}, \\ b &= 0.4, \\ B &= 1, \\ V &= v\frac{\mathrm{d}t}{\mathrm{d}x}. \end{aligned} \tag{7}$$

The absorbing velocity is v and is the velocity of the wavefront normal to the boundary. B and b are arbitrary constants. Values of 1 and 0.4, respectively, are suggested by Higdon (1991) and work well in many cases, but they may be modified to provide better absorption.

Two other types of boundaries include a reflecting boundary, where the displacement is set equal to zero, and a simple yet unconventional surface-perpendicular stress-free boundary, which we consider the free surface. The stress-free boundary has no surface-perpendicular displacement gradient. The displacement on the boundary is set equal to the displacement on the interior resulting in stress-free surface-perpendicular components. It is more common to set the normal and tangential stresses, containing both surface-parallel and surface-perpendicular components, to zero and solve the resulting equations. Whereas our method is stable for ratios of S- to P-wave velocity greater than 0.25, Vidale and Clayton (1986) present a method for applying a free surface boundary condition that achieves stability for ratios of S- to P-wave velocity greater than 0.02.

The final boundary condition, though not necessarily implemented on a boundary, is a specified condition and is usually used to specify the initial displacements on the boundary that are propagated into the model. This condition could be effectively used to minimize artifacts which commonly appear from the vertical sides of the model domain. For a non-vertically incident teleseismic wavefield, the bottom edge of the model toward the source will typically generate an additional wavefield that can interfere with interpretation, hence the need to

increase the width of the model domain. Application of this boundary on the vertical sides toward the source would eliminate this artifact. But due to the added complexity of having to determine reflectivity series and the resulting time series for each point along the vertical boundaries, this modification is not currently included.

These equations are implemented efficiently in Matlab in that the use of 'for' loops are minimized. Indexes to matrices are vectorized. This technique can lead to a significant reduction in processing time. For calculations involving 'for' loops and vectors with less than about 545 elements, processing time roughly doubles when the number of elements increases by a factor of 2 (Fig. 1A). For greater numbers of elements, calculation time increases more rapidly. Vectorized calculations however, show a very different trend. If the number of elements is doubled, processing time increases but by an amount far less than a factor of 2 (Fig. 1B), indicating that the actual calculation is not what requires much of the processing time. At about 545 elements, the processing time for vectorized calculations jumps by 30%, likely indicating the use of a different subroutine. For a vector with 100–1000 elements, the processing time required for looped calculations is 30–300 times greater than for vectorized calculations.

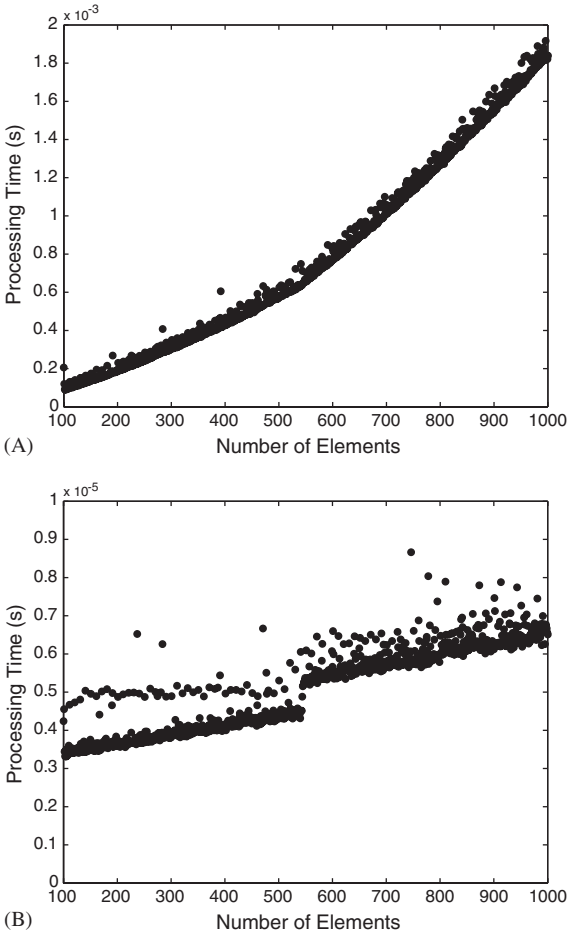

Fig. 1. Processing time of 'for' loops (A) and vectorized calculations (B) for varying vector sizes.

As an example of how the vectorized calculation is implemented in FDWaveAni.m, consider the second derivative of x-displacement, u, with respect to first, the y-direction and then to the z-direction,

$$\frac{\partial^2 u}{\partial y \partial z}(:,J,K) = \frac{u(:,J_>,K_>) - u(:,J_>,K_<) - u(:,J_<,K_>) + u(:,J_<,K_<)}{4dydz}, \tag{8}$$

where the colon, :, represents all indices along that dimension, J and K represent vectors of grid indices in the y- and z-direction, respectively, and the greater than and less than subscripts indicate a shift of those vectors to either side of the points in question. For example, if y varied from 1 to 5, e.g. 1, 2, 3, 4, 5, then the colon symbol would take on the values 1, 2, 3, 4, 5, J would be 2, 3, 4, $J_<$ would be 1, 2, 3, and $J_>$ would be 3, 4, 5.

3. Verification and discussion

We have verified the implementation of this solution by comparison with analytical solutions for simple cases. In the first test case, an isotropic structure is modeled for which is observed a primary arrival and various multiples (Fig. 2). In the second case, the structure has an anisotropic layer (Fig. 3).

For both cases, the model consists of 2 layers, a 90 km thick isotropic layer overlain by either an isotropic or anisotropic 30 km thick surface layer. Free surface boundaries are implemented on the top and sides and a gaussian source pulse with a dominant period of 5 s is propagated from the bottom. The grid spacing is 1 km and the sample interval is 0.1 s. A model that has $50 \times 50 \times 50$ nodes requires 509 MB of Ram and takes 2.08 s per time step on a Pentium 3.4 GHz under Matlab 7.0.1 and Windows XP.

Fig. 2 presents results for an isotropic medium with an impinging P-wave (A) and S-wave (B). The finite-difference results are given by the dashed lines, and the analytical results are given by the solid lines. In (A), the first two multiples can be seen within the time window shown, while in (B) only the first multiple is observed. The finite-difference and analytical solutions agree well. The finite-difference solution produces a slight asymmetry in the source pulse, which is due to grid dispersion. Reducing the grid spacing will result in less distortion but will require a shorter sampling interval to insure numerical stability. Fig. 3 presents results for an

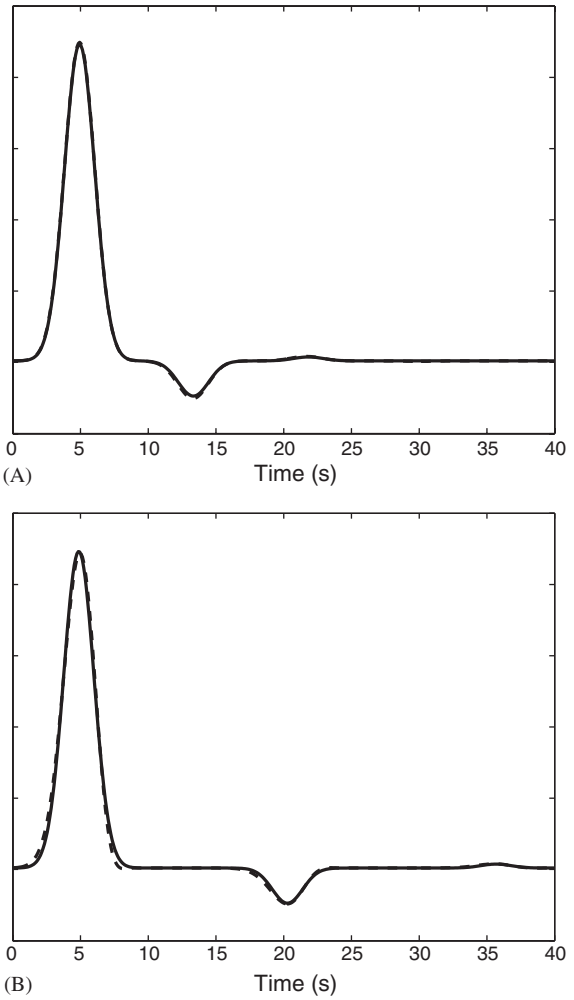

Fig. 2. Comparison of finite-difference solution (dashed) and analytical solution (solid) for a vertically incident P-wave (A) and S-wave (B) impinging on an isotropic layer. Arrival with negative polarity is first multiple.

anisotropic medium with an impinging S-wave. Our finite-difference solution also agrees well with the analytical prediction, but again suffers slight grid dispersion leading to the asymmetry in the seismic pulse.

This program has been used successfully to discriminate among possible isotropic structures in receiver function modeling (Boyd et al., 2005; Boyd and Sheehan, 2005b; Wilson et al., 2004; Zandt et al., 2004). For receiver functions, the vertical component seismogram is deconvolved from the radial component to remove complex source time series and reveal, ideally, the P- to S-wave conversions from subsurface impedance contrasts. This deconvolution is not necessary for our synthetics since the source time series is initially a

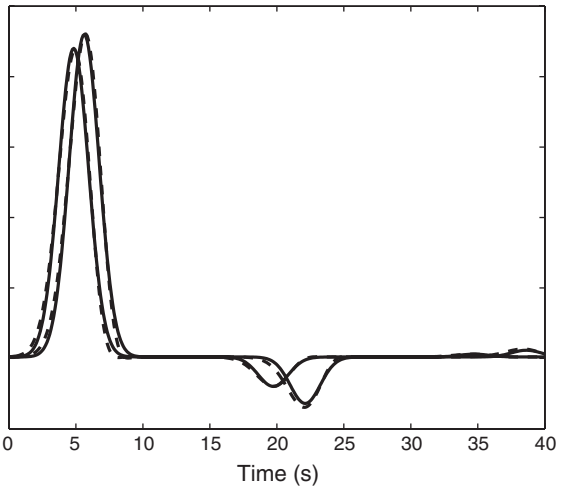

Fig. 3. Comparison of finite-difference solution (dashed) and analytical solution (solid) for a vertically incident S-wave impinging on an anisotropic layer. Negative arrivals are first S-wave multiples.

simple Gaussian. Standard receiver function techniques can be carried out however, to investigate the unwanted effects of deconvolving P-wave multiples from the radial component seismogram. The authors of the following examples use our code to calculate their synthetics and do not perform deconvolution to create their receiver functions.

Fig. 4 shows the synthetics generated by Wilson et al. (2004) to discriminate between a step or gradual ramp in the Moho beneath the northern South Island of New Zealand. The model is 500 km wide and 250 km deep with a node spacing of 500 m. This model requires 1.4 GB of memory and when run for 2600 time steps, takes on the order of 12 h to complete on a Sun Ultra 30 or 2 hours on a 3.2 GHz P4. Their receiver function stack strongly resembles the synthetics, which incorporate the same source-receiver geometry, having the Moho ramp and even includes the same significant artifacts due to non-uniform spatial sampling. Fig. 5 presents the modeling done by Zandt et al. (2004) to discriminate among candidate structures for the Moho beneath the southern Sierra Nevada. Based on their receiver function stack, they determined that a cusp on the Moho was more likely than either a series of steps or constant dip. In Fig. 6, synthetics were generated for a subduction zone structure to attempt to explain arrivals seen in both a common conversion point receiver stack (Boyd et al., 2005) and migrated receiver function stack (Boyd and Sheehan, 2005b) beneath the northern South Island of New Zealand. In both cases, the synthetic stacks strongly resemble the corresponding stacks made with real data.

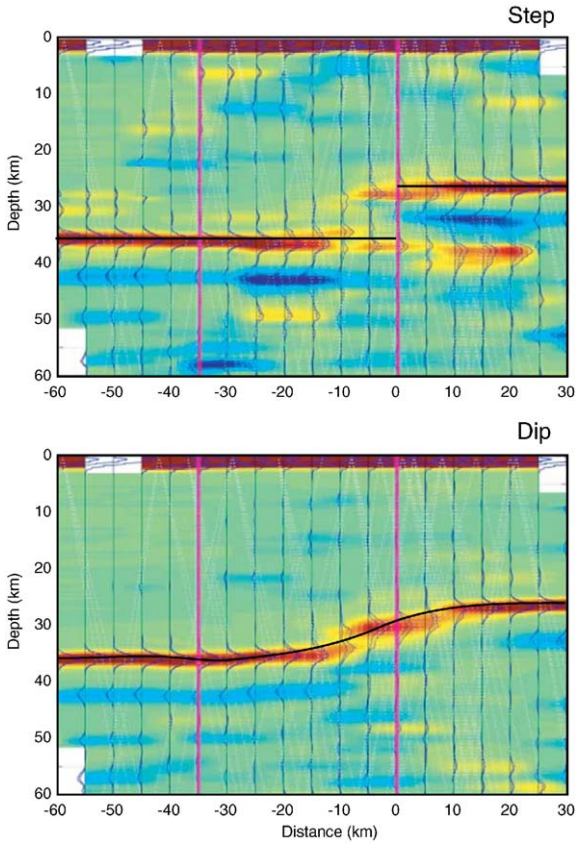

Fig. 4. Synthetic results using code developed in this paper for receiver functions in New Zealand (Wilson et al., 2004). Source–receiver geometry for real dataset was used as input to finite difference calculations. Top figure depicts a step in Moho at subsurface location of Wiarau fault whereas bottom depicts a constant dip across fault.

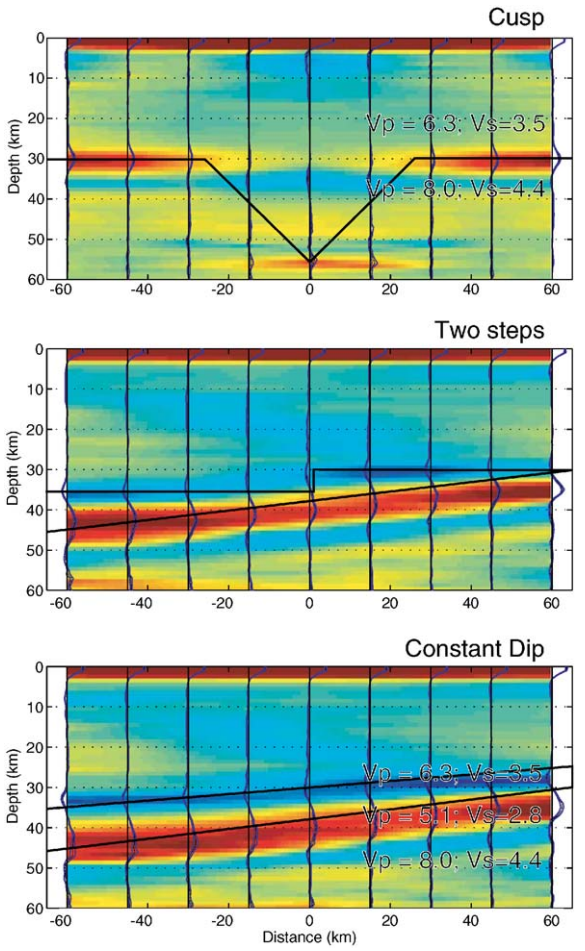

Fig. 5. Synthetic results using code developed in this paper for receiver functions beneath Sierra Nevada (Zandt et al., 2004). Source–receiver geometry for real dataset was used as input to finite difference calculations. Top figure depicts a cusp in Moho, middle, a step, and bottom, a constant dip.

The program has also been used to investigate the effects of frequency-dependent focusing and defocusing on the ability to measure seismic wave attenuation (Boyd and Sheehan, 2005a). Allen et al. (1999) noted that large seismic velocity gradients extending to several hundred kilometers depth can sufficiently bend low-frequency seismic rays to generate significant errors in estimates of attenuation. With this in mind, Boyd and Sheehan (2005a) used synthetics and the expected seismic velocity structure beneath the Colorado Rocky Mountains to find that, for their experiment, errors in attenuation due to ray bending would be negligible.

4. Conclusions

We have created a program to calculate second-order finite-difference synthetic displacement seismograms for heterogeneous anisotropic media in three dimensions. The solution is implemented in a Matlab script allowing greater interaction of the user with the temporally and spatially evolving wavefield. Matlab scripts are notoriously slow, especially when loops are introduced. We have minimized the use of loops and the resulting solution is efficient. Companion scripts are included which provide a framework for input to the finite difference solution as well as a routine to rotate the anisotropic tensors.

Our solution has been verified by comparison with simple analytical models. Computation time is reasonable allowing approximately 60 000 nodes to be computed per second in each time step on a 3.4 GHz Pentium CPU. Multiple applications of this program have been reported in which the authors were success-

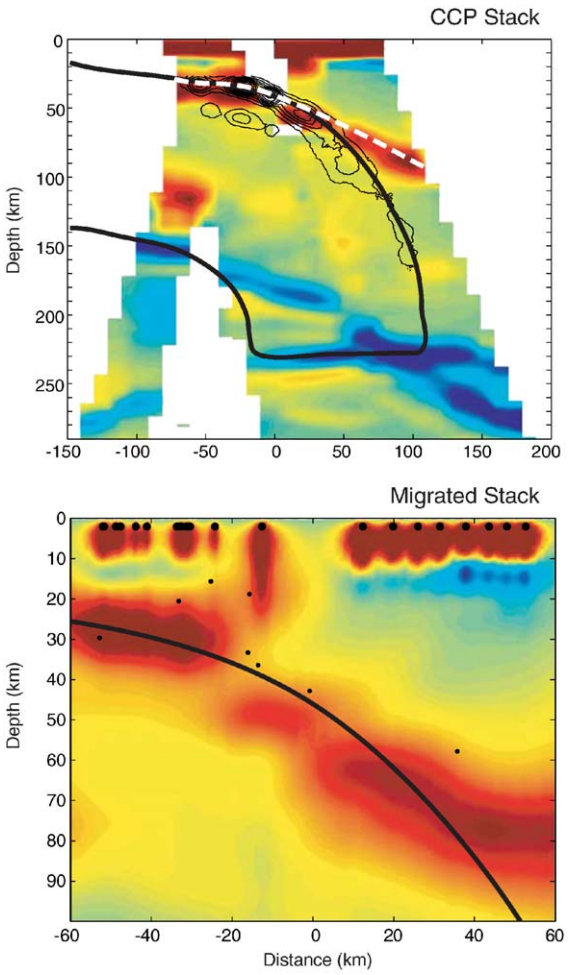

Fig. 6. Synthetic results from Boyd et al. (2005) (top figure) and Boyd and Sheehan (2005b) (bottom figure) using code presented in this paper. Both figures show effects of a subducting slab on common conversion point (CCP) and migrated receiver function stacks.

fully able to use the resulting synthetic seismograms to better interpret teleseismic data.

Acknowledgments

I gratefully thank Anne Sheehan for her encouragement and critical review of my work. I thank Charlie Wilson and Hersh Gilbert for providing feedback on the code and the figures that were part of their research. Two anonymous reviewers also helped to improve the manuscript.

References

Allen, R.M., Nolet, G., Morgan, W.J., Vogfjord, K., Bergsson, B.H., Erlendsson, P., Foulger, G.R., Jakobsdottir, S., Julian, B.R., Pritchard, M., Ragnarsson, S., Stefansson, R., 1999. The thin hot plume beneath Iceland. Geophysical Journal International 137, 51–63.

Babuska, V., Cara, M., 1991. Seismic-wave propagation in anisotropic media. In: Nolet, G. (Ed.), Seismic Anisotropy in the Earth. Kluwer Academic Publishers, New York, NY, pp. xx–yy.

Bohlen, T., 2002. Parallel 3-D viscoelastic finite difference seismic modeling. Computers & Geosciences 28 (8), 887–899.

Boyd, O.S., Sheehan, A.F., 2005a. Attenuation tomography beneath the Rocky Mountain Front: implications for the physical state of the upper mantle. In: Karlstrom, K.E., Keller, G.R. (Eds.), The Rocky Mountain Region: An Evolving Lithosphere. American Geophysical Union, Washington, DC, pp. 361–377.

Boyd, O.S., Sheehan, A.F., 2005b. Delineating slab structure beneath New Zealand by migrating receiver functions. Geophysical Research Letters, submitted.

Boyd, O.S., Savage, M.K., Sheehan, A.F., Jones, C.H., 2005, Illuminating upper mantle structure beneath Cook Strait, New Zealand, with receiver functions. Journal of Geophysical Research, submitted.

Frederiksen, A.W., Bostock, M.G., 1999. Modeling teleseismic waves in dipping anisotropic structures. Geophysical Journal International 141, 401–412.

Higdon, R.L., 1991. Absorbing boundary conditions for elastic waves. Geophysics 56 (2), 231–241.

Igel, H., Mora, P., Riollet, B., 1995. Anisotropic wave propegation through finite-difference grids. Geophysics 60 (4), 1203–1216.

Juhlin, C., 1995. Finite-difference elastic wave propagation in 2D heterogeneous transversely isotropic media. Geophysical Prospecting 43, 843–858.

Kelly, K.R., Ward, R.W., Treitel, S., Alford, R.M., 1976. Synthetic seismograms: A finite-difference approach. Geophysics 41 (1), 2–27.

Levander, A.R., 1988. Fourth-order finite-difference P-SV seismograms. Geophysics 53 (11), 1425–1436.

Shearer, P.M., 1999. The seismic wave equation. In: Shearer, P.M. (Ed.), Introduction to Seismology. Cambridge University Press, Cambridge, pp. 25–34.

Vidale, J.E., Clayton, R.W., 1986. A stable free-surface boundary condition for two-dimensional elastic finite-difference wave simulation. Geophysics 51 (12), 2247–2249.

Wilson, C.K., Jones, C.H., Molnar, P., Sheehan, A.F., Boyd, O.S., 2004. Evidence for continuous deformation in the lower crust and upper mantle beneath a continental strike-slip fault zone: Marlborough Fault System, South Island, New Zealand. Geology 32 (10), 837–840.

Zandt, G., Gilbert, H., Owens, T.J., Ducea, M., Saleeby, J., Jones, C.H., 2004. Active foundering of a continental arc root beneath the southern Sierra Nevada in California. Nature 431, 41–46.